Geophysical Research Letters

RESEARCH LETTER
10.1029/2019GL082986

Wavelet-Based River Segmentation Using Hydraulic Control-Preserving Water Surface Elevation Profile Properties

A. Samine Montazem[1,2], P-A. Garambois[2], S. Calmant[1], P. Finaud-Guyot[3], J. Monnier[4], D. Medeiros Moreira[5], J. T. Minear[6], and S. Biancamaria[1]

[1]LEGOS, Laboratoire de Géophysique et Océonagraphie Spatiale, Toulouse, France, [2]INSA Strasbourg, ICUBE, Fluid Mechanics Team, Strasbourg, France, [3]ENGEES, ICUBE, Fluid Mechanics Team, Strasbourg, France, [4]Mathematics Institute of Toulouse, Toulouse, France, [5]CPRM, Companhia de Pesquisa de Recursos Minerais, Brasilia, Brazil, [6]CIRES/University of Colorado, Boulder, CO, USA

Key Points:
- The hydraulic visibility of river surface profile variabilities from space is investigated
- Hydraulic control signatures are depicted in local extrema of water surface curvature
- A wavelet-based river segmentation preserving hydraulic controls is proposed

Correspondence to:
A. Samine Montazem,
amanda.montazem@legos.obs-mip.fr

Citation:
Samine Montazem, A., Garambois, P.-A., Calmant, S., Pascal, F.-G., Monnier, J., Medeiros Moreira, D., et al. (2019). Wavelet-based river segmentation using hydraulic control-preserving water surface elevation profile properties. *Geophysical Research Letters*, *46*, 6534–6543. https://doi.org/10.1029/2019GL082986

Received 28 MAR 2019
Accepted 17 MAY 2019
Accepted article online 28 MAY 2019
Published online 19 JUN 2019

Abstract River flow models that consider satellite observations of the water surface elevation (WSE) require meaningful segmentation into reaches. Segmentation methods involve a trade-off between the spatial sampling and error characteristics of satellite observations, both of which impact the flow model realism/accuracy. This paper investigates the spatial properties of WSE profiles (slope and concavity) and their link with hydraulic controls (HCs) and leverages this knowledge to advance river segmentation. Fine-scale synthetic cases were analyzed to characterize HC effects on the remotely observable WSE properties. Following this, a wavelet-based segmentation method was developed and subsequently tested on real rivers, including test cases with measurements characteristic of the Surface Water and Ocean Topography satellite mission. The results show that the local extrema of water surface (WS) concavity are good candidates for defining reach bounds while consistently preserving the HC signatures and local flow nonuniformities (deviations from equilibrium) from fine to large spatial scales.

1. Introduction

Remote sensing techniques offer promising measurement capabilities for hydrological sciences (Biancamaria et al., 2016). Based on the current observation scales of satellite altimetry (Alsdorf & Lettenmaier, 2003; Calmant & Seyler, 2006), few hydraulic studies of river surface profiles have been proposed. O'Loughlin et al. (2013) studied 1,600 km of the middle Congo, evaluating possible locations for hydraulic control (HC) sections (local deviations to equilibrium) based on WS width observations (Landsat imagery) and three seasonal WS elevation and slope profiles derived from IceSat measurements. With six ENVISAT virtual stations along 70 km of the Xingu River, Garambois et al. (2017) found that HCs could be identified and characterized from WS elevations. The latter introduced the concept of "hydraulic visibility" of the WS slope and concavity variations and spatiotemporal nonuniformities that are shown to depend heavily on the spatial resolution and extent of the observations. The upcoming Surface Water and Ocean Topography (SWOT) satellite mission is designed to observe river WS elevation and extent quasi-globally, with an unprecedentedly fine spatial coverage (Rodriguez, 2012). Several studies have investigated the benefits of using SWOT-like data for constraining river flow models (see Biancamaria et al., 2016, for a review). The discharge estimation is addressed in those studies with forward and inverse hydraulic models, mostly using daily WS elevations averaged on deca-kilometer reaches, chosen primarily to reduce the random errors expected from the SWOT sensor, plus ancillary data (unobservable river bathymetry and friction). The importance of balancing the flow model complexity and the spatiotemporal scales of the WS measurements and hydraulic information content is highlighted by Garambois and Monnier (2015) and Brisset et al. (2018). In this context, which compromise among the reach lengths (segmentation), data accuracy, and hydraulic behavior scaling is most appropriate in light of the complexities and goals of forward and inverse modeling?

The HCs locations can be detected by the WS concavity variations and can be used to segment a river into successive reaches (Garambois et al., 2017). WS inflection points along with the river centerline sinuosity were recently used by Frasson et al. (2017), with additional reach breaks at tributaries, to define reaches of more

than 5 km using simulated SWOT observables on individual river snapshots. By applying the WS inflection method to two river portions of about 130 km in length, they found that the reach-averaged forward discharge calculations using the Manning equation produce less than an 11% error in the observed discharge. These reach segmentation methods are found to produce better reach-averaged slopes compared to those of arbitrary deca-kilometric reaches. Nevertheless, a more comprehensive investigation of the impacts of reach definition is needed to improve the river segmentation methods. In this paper, we seek to address this need.

The flow momentum balance varies along a river because of several factors including variations in channel geometry, flow resistance, discharge, and lateral fluxes. In the context of rivers surfaces remote sensing, the flow depth variations that stem locally from the equilibrium between the driving forces and flow resistance are still unobservable, and some question arise:

- What is the hydraulic visibility of WS profile nonuniformities from satellite altimetric missions?
- What is the impact of segmentation on the hydraulic signal, and which method enables the best reproduction of the main flow features?

The objectives are to (1) develop a physically based river segmentation method tailored for satellite detection scales while best preserving essential hydraulic information for accurate modeling and (2) better understand the effects of a segmentation on the modeled flow lines. First, we discuss hydraulic theory as it applies to WS observations, and second, we use this theory to develop a large set of synthetic test cases. The visibility of the fluvial HCs from the WS curvature variability is investigated in detail for those fine-scale synthetic cases and a "hydraulic-preserving segmentation" method is proposed. Third, we evaluate the segmentation methods on real cases.

2. HCs and River Network Segmentation

2.1. Governing Equations and Physical Hypotheses

Open-channel flows are commonly described with the 1-D Saint-Venant equations involving an integration of the flow variables over the cross-section (e.g., Chow, 1959). The typical space-time scales of satellites allow the observation of locally gradually varying steady state flows described by the backwater curve equation: $\left(1-\mathrm{Fr}^2\right)\partial_x h = I - J_1 + J_2$, with h the flow depth (m), $I = -\partial_x Z_b$ the bed slope (m/m), Z_b the bed elevation (m), $J_1 = \frac{Q^2}{K^2 A^2 R_h^{4/3}}$ the energy slope due to bottom friction (m/m)], J_2 the energy slope due to width variations (m/m), $\mathrm{Fr} = \sqrt{\frac{Q^2 W}{gA^3}}$ the Froude number, Q the discharge (m^3/s), W the WS width (m), K the Strickler roughness coefficient ($m^{1/3}/s$), g the gravity acceleration (m/s^2), A the wetted cross-sectional area (m^2), and $R_h = \frac{A}{P}$ the hydraulic radius (m) with P the wetted perimeter (m). The synthetic cases are simulated with rectangular cross-sections leading to $J_2 = \mathrm{Fr}^2 \frac{h}{W}\partial_x W$.

2.2. Fluvial Hydraulic Profiles and Downstream Control

The classification of hydraulic steady state gradually varying flows in prismatic channels, for a given roughness and discharge, categorizes flow configurations with respect to the longitudinal profiles of the WS and channel bottom into horizontal, mild, critical, steep, or adverse slopes (Chow, 1959). For each class, up to three configurations are possible depending on the water depth at the HC location compared to the normal depth h_n and critical depth h_c. In prismatic channels, the normal depth corresponds to the equilibrium between the gravitational traction and friction drag. Extending the definition of h_n for nonprismatic channels while preserving the equilibrium property yields a normal depth that corresponds to the equilibrium $I - J_1 + J_2 = 0$ including the lateral pressure force. The critical depth corresponds to the transition between supercritical ($Fr > 1$) and subcritical ($Fr < 1$) regimes.

Satellite altimetry mostly observes the downstream parts of river networks (>100 m for SWOT), mainly in subcritical (and mostly low Froude) flows with mild (M) or adverse (A) slope classes. The fluvial HCs can be defined as the locations of the maximal deviations of the depth from the normal depth h_n, imposing the upstream variation of the water depth profile $h(x)$ over the so-called control length (cf. Samuels, 1989; Figure 1). The HCs in a channel can be due to changes in at least one of the following parameters: the hydraulic resistance, cross-section shape, and bottom slope. They are responsible for the nonuniform variations of the WS profile Z and its spatial derivatives: WS slope $\partial_x Z$ and concavity $\partial_x^2 Z$ observable; see profiles from along flow nadir altimetry measurements in Garambois et al. (2017). A detailed investigation of fluvial HC signatures in WS variabilities is presented hereafter.

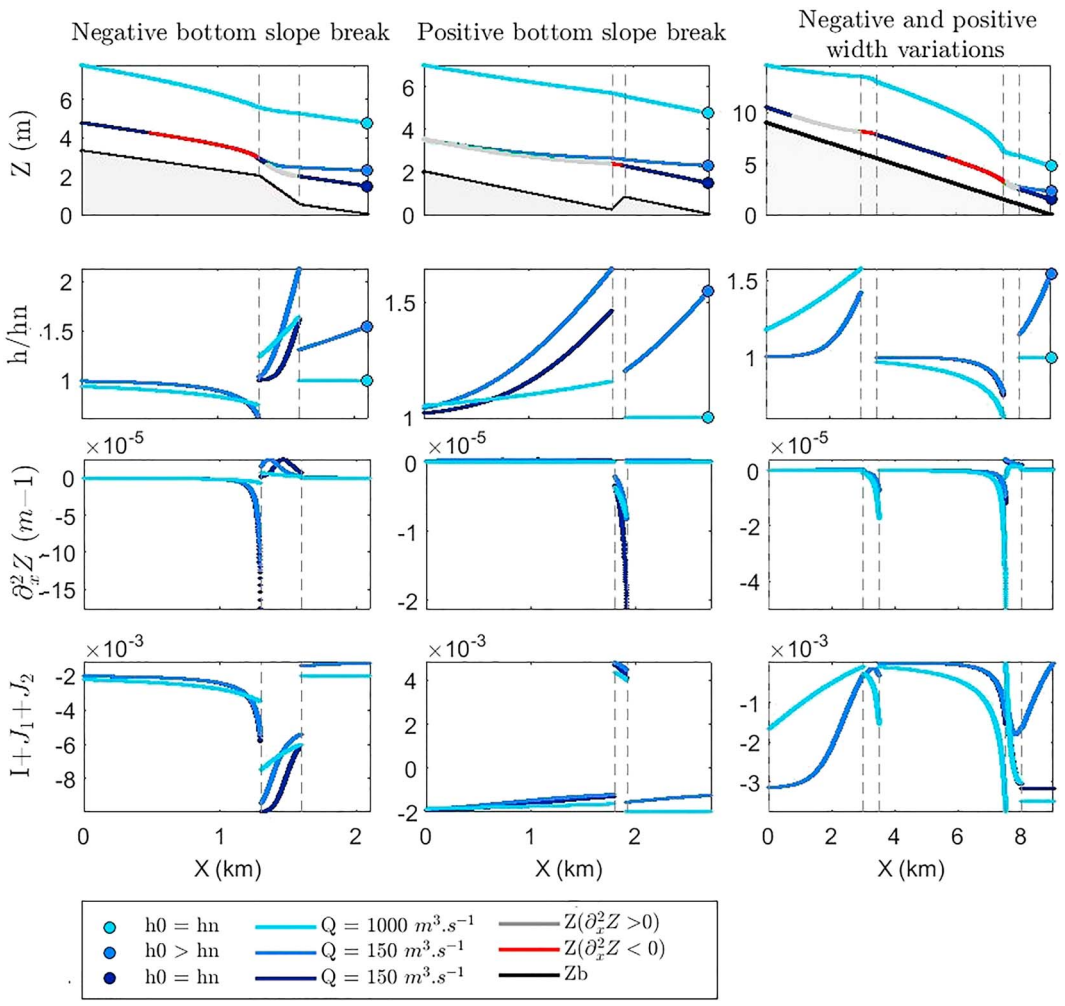

Figure 1. Elementary basis decomposition of channel variabilities with a constant roughness ($K = 25\ \mathrm{m}^{1/3}/\mathrm{s}$). Dashed vertical lines correspond to reach bounds. Column 1: negative bottom slope break varying from -1.10^{-3} to -5.10^{-3} m/m. Column 2: positive bottom slope break varying from -1.10^{-3} to 5.10^{-3} m/m. Column 3: negative width variation varying from $W = 100$ m to $W = 50$ m followed by a positive width variation from $W = 50$ m to $W = 100$ m on a bottom slope of -1.10^{-3} m/m. Line 1: WS elevation Z. Line 2: deviation to the normal depth h/h_n. Line 3: WS curvature $\partial_x^2 Z$. Line 4: force term weights. WS curvature $\partial_x^2 Z < 0$ is highlighted in red and $\partial_x^2 Z > 0$ in gray for only dark blue profile for better readability.

2.3. Multiscale Analysis of HC Signatures in Synthetic Cases

The HCs and their associated WS deformations, slope, and concavity are studied here for several combinations of typical channel geometries, (low and high) flow regimes, and downstream boundary conditions. Synthetic channel geometries with uniform roughness are defined with either positive and negative bottom slope breaks $\partial_x Z_b$ and channel width variations $\partial_x W$ (Figure 1, line 1).

The backwater curve equation $\left(1 - \mathrm{Fr}^2\right) \partial_x h = I - J_1 + J_2$ describes the depth variabilities of permanent flows as the equilibrium $I - J_1$ between the bottom pressure, friction, and the unclassical J_2 due to width variations. This ordinary differential equation is solved using a finite difference method from a water depth imposed downstream (fluvial), which gives access to all the flow variables. Figure 1, line 4, shows that the variation and magnitude of the source term $I - J_1 + J_2$ along the flow is negligibly impacted by the flow regime. For the width-varying case $I = 10^{-3}$, at a low flow $J_1 \in [9.10^{-4}; 4.10^{-3}]$ and $J_2 \in [-3.10^{-4}; 6.10^{-4}]$ while for a high flow $J_1 \in [1.10^{-3}; 4.10^{-3}]$ and $J_2 \in [-1.10^{-3}; 3.10^{-3}]$. In that case, the energy slope J_2 due to width variations is on the order of I and J_1. This highlights the importance of considering a normal depth h_n based on the equilibrium of the bottom pressure (I), friction (J_1), and lateral pressure terms (J_2) for worldwide river hydraulic characterization.

We show in Figure 1, line 2, that for all cases, the reach control sections, that is, the largest deviations of h to h_n, are located at the downstream end of a (prismatic) reach. For subcritical regimes, the magnitude of those deviations is locally controlled by the upstream flow depth of the downstream reach or the imposed boundary condition. Depending on the reach control, h will tend to h_n (by superior or inferior values) upstream. For a real river domain, several HCs of various degrees of importance and backwater lengths can exert effects. Consequently, the WS slope $\partial_x Z$ is a priori different from the bottom slope $\partial_x Z_b$, that is, nonuniform flow zones (Figure 1, line 2, $h/hn \neq 1$).

We intend to characterize the HCs from the capabilities of current and future spatial WS observables. We use the WS elevation Z and its spatial derivatives $\partial_x^n Z = \partial_x^n h + \partial_x^n Z_b$, $n = 1, 2$ instead of the water depth that is unobservable from space. For all the tested configurations, it appears that $\partial_x Z < 0$ and $\partial_x^2 Z \in \mathbb{R}$ (Figure 1, lines 1 and 3). The curvature extrema appear to be close to the reach bounds. Indeed, on the tested configurations, the sign of $h/hn - 1$ is the same as the sign of the curvature (cf. Figure 1, lines 2 and 4); a positive sign corresponds to an M1 slope class, whereas a negative sign corresponds to an M2 or A2 slope class. We use the following convention for depicting on the flow profile concave portions ($\partial_x^2 Z < 0$) in red and convex portions ($\partial_x^2 Z > 0$) in gray. The results show that local curvature extrema appear at or upstream of the HCs, with the strongest curvature extrema indicating the strongest control at the domain scale. Therefore, the local extrema of the WS curvature are a good indicator to depict the location of the HCs.

Note that HCs due to bottom slope breaks (Figure 1, columns 1 and 2) are more identifiable during low flows because the WS curvature is more pronounced than during high flows, while those due to width variations (Figure 1, column 3) are more identifiable for high flows than for low flows for identical reasons.

2.4. Segmentation Method Based on Hydraulic Visibility

Because WS variabilities appear from fine to large spatial scales, the WS observables and especially the $\partial_x^2 Z$ extrema reflecting the main HCs as evidenced above are isolated through wavelet processing. Using wavelets (e.g., Mallat, 2008) to decompose a WS signal offers the possibility to do it at the scale of a river snapshot of varying length while obtaining spatially localized frequential information. This property therefore enables the identification of local WS undulations due to hydraulic signatures and also powerful signal denoising.

The WS profiles are decomposed using a continuous wavelet transform with the Paul wavelet (Torrence & Compo, 1998) because it leads to the best statistics in terms of signal reconstruction and the smallest « artificial » oscillations. WS signals are classically filtered by removing wavelet coefficients for increasing cutoff wavelengths λ_c and then recomposing them. Next, the WS slope and curvature are calculated by spatial finite differences on the filtered WS elevation signal. A river segmentation is finally obtained, its "spatial resolution" being imposed by a given λ_c, using as reach bounds the curvature extrema or annulation points (inflections of $Z(x)$) remaining in the filtered signal. Three segmentation strategies are investigated:

1. Reach boundaries defined by the local curvature extrema of the WS (HC);
2. Reach boundaries defined by the inflection points of the WS (IP);
3. Reach of constant length (CL).

The segmentation strategies are tested hereafter on perfect and noisy WS profiles, and the impact of λ_c on reach lengths and on the detection of the HCs (equivalently reach bounds) is assessed. The influence of a river segmentation on the simulated hydraulic variables, at the resolution imposed by the segmentation, is also assessed since it is of prior interest in the context of (inverse) river modeling from WS observables. The backwater curve equation is solved on a segmentation grid with (1) real values of the discharge Q, cross-section shapes and Z_b attributed at the reach boundaries and linearly interpolated from one reach to the other and (2) a constant roughness and no lateral inflows.

3. Results

3.1. Evaluation of Segmentation Strategies on a Well-Documented Case: The Garonne River

3.1.1. Perfect WS Observations

A 76-km reach of the Garonne River is used with the river bathymetry (Larnier, 2010; Simeoni-Sauvage, 1999) described from 173 in situ cross-section measurements at distances of 56–2,200 m and densified by linear interpolation. We use daily flow lines simulated with a 1-D hydrodynamic model (HEC-RAS); the discharges range from 40 to 890 m^3/s (year 2010). To select a statistically observable low-flow profile (HC visibility), the first quartile of the cumulative average daily flow distribution is selected ($Q = 83.9\ m^3/s$).

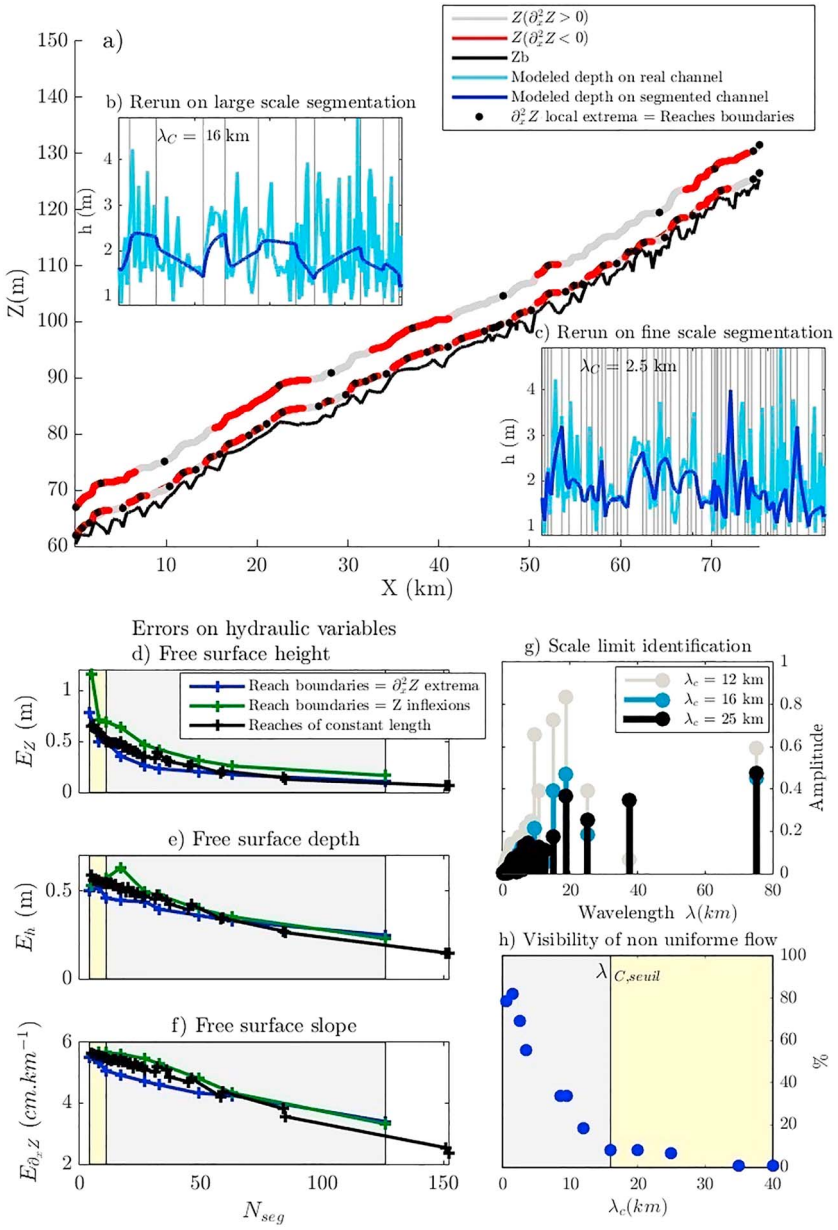

Figure 2. (a) Fine-scale segmentation on real WS height profile of the Garonne River with $\lambda_c = 2.5$ km. Large-scale segmentation on the same profile (shifted 7 m from true height) with $\lambda_c = 16$ km. Flow depth h simulated (blue) on the (b) fine-scale segmentation and (c) large-scale segmentation compared to the true depth profile (red). (d) Mean error on WS height. (e) Mean error on depth. (f) Mean error on WS slope. (g) Spectral analysis of the slope of the filtered WS height for $\lambda_c = 12, 16, 25$ km. (h) Percentage of the domain for which the WS slope varies by more than 10% of the bottom slope. Yellow zones of (c)–(e) correspond to $4 < number\ of\ reaches < 11$ (equivalent to 40 km $> \lambda_c >$ 16 km) and gray zones to $11 < number\ of\ reaches < 132$ (16 km $> \lambda_c >$ 0.5 km). $\lambda_c = 0.5, 1.5, 2.5, 3.5, 4.5, 5.5, 6.5, 7.5, 8.5, 9.5, 12, 16, 20, 25, 35, 40$ km.

For the constant length segmentation, 80 reach lengths ranging over [0.2, 16] km by steps of 200 m are considered with 50 random starting points (4,000 segmentation grids). For both segmentation methods based on hydraulic considerations (HC, IC) we applied a low-pass filter of a cutoff wavelength $\lambda_c \in [0.5; 40]$ km.

Figure 2a shows a fine-scale segmentation (HC) into 49 reaches resulting from $\lambda_c = 2.5$ km and a large-scale segmentation into 11 reaches resulting from $\lambda_c = 16$ km. The performances of the three segmentation methods are then evaluated in terms of the discrepancy E_p between the true flow line (Z_{true}) and those simulated on the coarser segmentation-based subsamplings (Z_{sim}) such that $E_p = \frac{1}{N}\sum_{i=1}^{N} |p_{sim_i} - p_{true_i}|$, $p = \{Z, \partial_x Z, h\}$.

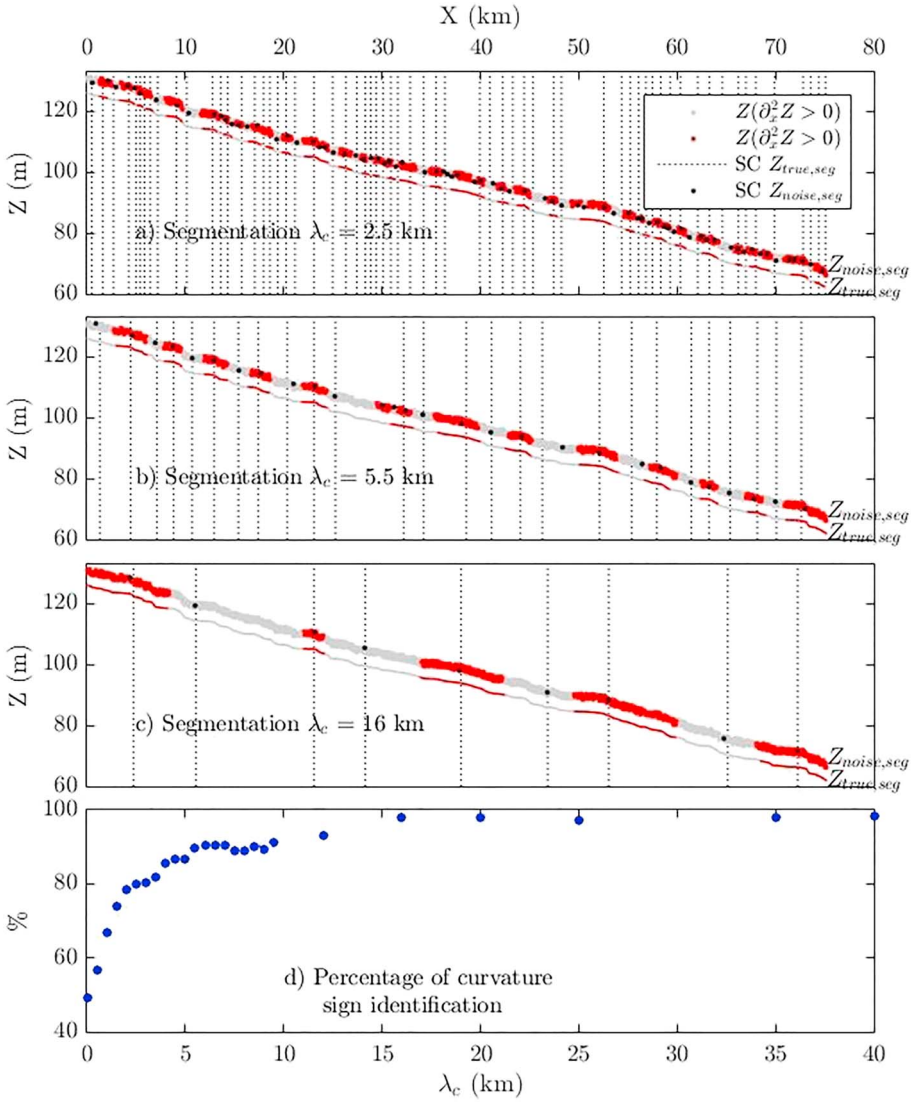

Figure 3. Segmentations for increasing λ_c on noisy river profiles obtained by adding a random Gaussian noise $\sigma_Z = N(0, 1) = [-1, 1]$ m at the 200 m model grid resolution to the true WS elevation signal on the whole spatial domain D as $Z_{noised}(x) = Z_{true}(x) + \sigma_Z(x)$, $\forall x \in D$. (a) Segmentation with $\lambda_c = 2.5$ KM. (b) Segmentation with $\lambda_c = 5.5$ km. (c) Segmentation with $\lambda_c = 16$ km. (d) Spatial percentage P_c of curvature signs remaining in the filtered noisy signal (with respect to filtered true signal) at the scale of the domain.

The quality of a segmentation is assessed by plotting the error $E_p(N)$ in function of N the number of reaches (Figures 2d–2f). Unsurprisingly, refining the segmentation decreases the error of the model based on this segmentation grid, hence improving the model realism compared to the reference flow profile and especially the preservation of HCs. $E_p(N)$ for the WS elevation, depth, and slope is systematically lower for the proposed HC segmentation method based on the local extrema of the curvature (associated with the strongest controls).

Two zones of variation of $E_p(N)$ are highlighted (in yellow and gray) in Figures 2d–2f. The effect of the segmentation scale λ_c is depicted by a spectral analysis of the slope of the filtered WS profiles. We show in Figure 2g that for $\lambda_c > 16$ km the principal harmonic of the slope mostly corresponds to large-scale river shape properties. Moreover, increasing the reach lengths leads to decreased visibility of the nonuniform flow zones. This is evidenced in Figure 2h in terms of the deviation of $\partial_x Z$ to $\partial_x Z_b$. For segmentation resulting from $\lambda_c > 16$ km (gray zone) less than ±10% of the resimulated WS slope is different from the river bottom slope for this 76-km river portion, yet it is characterized by relatively high slope values and variabilities. In

other words, only locally uniform flows ($h = h_n$) are visible when looking at a river with a relatively large spatial stencil (compared to river width).

In conclusion the segmentation method based on WS curvature extrema enables the definition of reaches preserving the HCs. This is crucial for setting up hydraulic models that are coherent with the real flow profile and the informative content of WS observables.

3.1.2. Noisy WS Observations

A noisy river profile is obtained by adding to a reference WS profile Z_{true} a random Gaussian noise $\sigma_Z = N(0,1) = [-1;1]$ m at the 200-m model grid resolution, which is coherent with the expected SWOT measurement errors (cf. Rodriguez, 2012): $Z_{noised}(x) = Z_{true}(x) + \sigma_Z(x), \forall x \in \mathcal{D}$ where $\mathcal{D}$ is the spatial domain. The HC segmentation method is applied to the noised profiles exactly as done previously using a low-pass filter of a cutoff wavelength $\lambda_c \in [0.5; 40]$ km.

Three segmentations obtained by increasing values of λ_c are presented in Figure 3; $\lambda_c = 2.5$ km results in 64 segments of a 1.17-km mean length. In that case, the spatial percentage P_c of correct curvature sign remaining in the filtered noisy signal (with respect to the filtered true signal) at the scale of the domain equals 78%. When increasing λ_c to 5.5 km, $P_c = 91\%$ ($\lambda_c = 16$ km, $P_c = 98\%$), meaning that a higher percentage of the curvature sign of the domain are identified at a larger scale and hence more filtering cutoff scale. These λ_c values also correspond to larger and hence less numerous reaches of mean length, respectively, on the order of 2.9 and 8.3 km. Remarkably, the location of the HCs, and hence reach bounds (black points), detected in the noisy SWOT-like signal are in very good agreement with the ones obtained on the true WS (dashed lines). This highlights the efficiency of wavelets in dealing with noisy data without creating unphysical oscillations. Note that the largest-scale segmentation preserves nearly exactly the strongest and most significant HCs despite the measurement noise. Moreover, layover may bias the SWOT WS locally (Domeneghetti et al., 2018), which is not considered in this study but should have a limited impact on HCs detection with our method, especially if the WS curvature remains visible and correct.

3.2. HC Visibility and Segmentation of an "Ungauged" Case: The Negro River

The segmentation method is applied to four in situ longitudinal WS profiles (GPS) of 1,000 km of the Negro river (a major Amazon tributary): two in low flows (October 2010) and two in high flows (September 2009) collected by survey ships (cf. Moreira et al., 2016). At their confluence, the discharges of the Negro River and the upstream Amazon (Solimoes) usually range between [4,200, 50,000] m^3/s and [68,000, 130,000] m^3/s, respectively; the WS height interseasonal variability shows a 12-m amplitude (Figure 4).

Because the Amazon Basin extends on both sides of the equator, these rivers are subject to different hydrological regimes, and the low-flow regimes of the Negro River and the Solimoes River are out of phase (Meade et al., 1991). A strong backwater effect appears as clearly depicted by the three GPS profiles obtained for the higher flow regimes. During the flood period of the Solimoes River, the high water elevation at the confluence induces a strong downstream control on the Negro River. This backwater effect (as shown in synthetic cases in Figure 1, column 1, mild blue) propagates far upstream and the WS is clearly flattened. The backwater length depends on the Negro River discharge itself and on the water depth at their confluence.

The Fourier spectra of the slope of the lowest flow profile are presented for three filtering lengths λ_c (Figure 4, profile 1). Indeed, this profile is more sensitive to fine-scale channel geometry variations because of the smallest backwater effect induced by the confluence. For a highly filtered or equivalently coarsely segmented WS signal, again, most of the spectral density of the slope is carried by large-scale features for $\lambda_c = 30$ km. We present hereafter a large-scale segmentation with $\lambda_{c2} = 150$ km (Figure 4d) enabling the highlighting of the large WS curvature scales caused by the main HCs.

For the upstream zone affected by neither the confluence backwater effect nor the large-scale width variations between $X = 650$ km and $X = 1,000$ km, the four segmented profiles are similar. The small differences in the reach bound positions are due to low- and high-flow conditions. At the bottom slope breaks located at $X = \{770; 825; 881\}$ km, the sign of the WS curvature changes from negative to positive, which is consistent with the synthetic test cases in Figure 1, column 1.

The downstream parts of profiles 2–4 are forced by the backwater effect resulting in a large-scale convexity ($\partial_x^2 Z > 0$) of the WS. The location of the WS curvature extrema varies from $X = 183$ km for profile 2 to $X = 297$ km for profile 3 and up to $X = 514$ km for profile 4. At $X = 351$ km the segmentation highlights

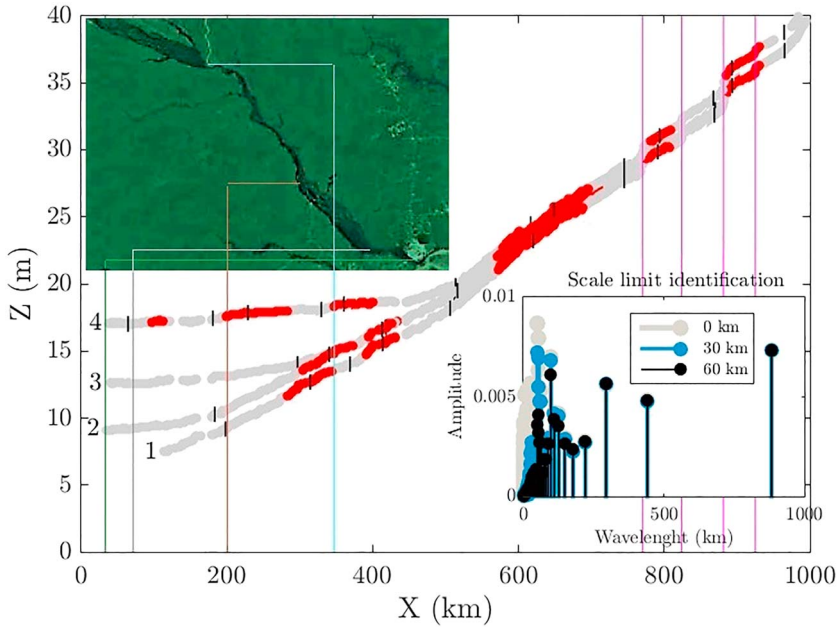

Figure 4. Longitudinal water height profiles of the Negro River for contrasting flow regimes. The channel of the Negro River is marked by seven large-scale channel variations (indicated by vertical lines): a width contraction located at $X = 71$ km, a width enlargement at $X = 200$ km, a width contraction combined to the confluence with the Branco River at $X = 351$ km, and four slope breaks located at $X = 770$, $X = 824$, $X = 881$, and $X = 825$ km, X being the distance in kilometers from the confluence with Solimoes River. Large-scale segmentation with $\lambda_c = 150$ km. Landsat mosaic by Google Earth highlights Manaus at $X = 36$ km and the width variations described above at $X = 71$, $X = 200$, and $X = 351$ km. Subfigure right: spectra of the WS slope signals for different filtering lengths of profile 1 (we only represent $\lambda_c = 0$ km, $\lambda_c = 30$ km, and $\lambda_c = 60$ km for better readability).

the effect of the width contraction of the channel, at the confluence with the Branco River, on the upstream flow line (Figure 4, vertical blue line). The effect of this HC is characterized by a sign reversal of the WS curvature, from positive to negative, around the HC, which is consistent with the flow analysis on synthetic channels (Figure 1, column 3). For high flow, the backwater control at $X = 351$ km propagates upstream of this control section (profile 4 red zone). Interestingly, as demonstrated for the synthetic test cases with the influence of J_2, a HC appears for high flow at $X = 200$ km (Figure 1, columns 1 and 3) probably because of sudden river enlargement.

4. Discussion

This paper studies the correlation between the spatial variabilities of river flow surface observables (WS elevation, slope and curvature) and the longitudinal variations in the channel bottom and width variabilities. As a matter of fact, the 1-D steady state shallow water equations (section 2.1) rely on several hypotheses (cf. Chow, 1959) including the averaging of the hydraulic variables on each cross-section and do not account for channel sinuosity.

The HCs corresponding to maximal deviations of h to h_n are characterized at fine scales by maximal WS slopes and related at all scales to local curvature extrema. Consequently, such proxies are suited for defining reach bounds since they impose flow line behavior upstream in the fluvial regimes of interest.

The WS curvature inflection points (sign reversal) used by Frasson et al. (2017) to define the bounds of large reaches may be difficult to relate to the HCs. Indeed, as shown in the synthetic and Garonne cases (Figures 1 and 2), WS profile inflection points can appear in the middle of a riffle or a pool or for uniform flow zones and at a scale larger than that for a single HC. Therefore, inflection points are not necessarily related to HCs. The use of local curvature extrema, which are related to the strongest HCs of a reach (for all scales), results in accurate flow profile modeling, as found above, and consequently a better coherence of the modeled flow line with respect to observables. Moreover, curvature extrema may be more visible in a noisy signal than

inflections corresponding to null values. Note that our wavelet-based method enables both filtering and segmenting the signal thanks to wavelet properties, as shown for two real cases with noisy observations.

Importantly, using a relatively coarse segmentation, that is, with reaches longer than the HC lengths, results in depicting only locally uniform flows ($h = h_n$). Preserving this hydraulic visibility of flow nonuniformities could be of importance for hydraulic modeling, especially for performing an optimal combination of satellite measurements and river models via data assimilation.

Considering GPS profiles of the "ungauged" Negro River, the visibility of the HCs is linked to the WS behavior characterized for the synthetic cases (section 2.3). Important width gradients and slope breaks are indeed identified thanks to WS curvature signal. The temporal variability of the downstream control at the Negro-Solimoes confluence is shown to create a backwater effect up to 650-km upstream. The WS curvature is also shown to be correlated with large-scale channel variations and downstream control highlighting the relevance of the proposed segmentation method to identify HCs.

5. Conclusion

From synthetic hydraulic cases to 76-km snapshots of the Garonne River with SWOT-like measurement errors and 1,000 km in situ WS GPS profiles in the Amazon Basin, this paper investigates river segmentation from WS observables in light of HCs and their visibility from space.

Through representative synthetic cases the link between the WS local extrema of the curvature and the local deviations to the normal depth h_n characterizing HCs is clearly highlighted. h_n is redefined here as the equilibrium between the longitudinal and lateral influences in the context of remote sensing. Next, the wavelet-based segmentation from WS observables nicely enables both noise filtering and HC detection at various scales through the identification of the WS curvature extrema. The resulting reaches allow a good hydraulic representation of segmented rivers.

Real flow profiles contain fine hydraulic signals that satellites such as SWOT should be able to depict. Indeed, it is demonstrated on the Garonne and Negro Rivers that increasing the segmentation length quickly reduces the visibility of flow nonuniformities hence only depicting uniform flow reaches. Consequently, a segmentation length threshold should not be exceeded to preserve the small-scale HC signatures containing precious hydrodynamic information. Moreover, we have shown that the temporal variability of the segmentation has to be considered, especially for reaches affected by backwater effects or by geometric width variations at high flows.

The proposed segmentation method based on WS observables only is applicable to ungauged river snapshots as those expected from SWOT. It is shown to produce an "effective" longitudinal channel and hydraulic variability preserving the main HCs, which might be of prior interest for coupled hydraulic-hydrology (inverse) problems. Ongoing works investigate the hydraulic signal visibility in space and time considering SWOT spatiotemporal pattern and river/flow classifications.

Acknowledgments
The authors acknowledge the Centre National d'Etudes Spatiales and the University of Toulouse for funding the first author, the Tosca-CNES that benefited all the French authors, and the Companhia de Pesquisa de Recursos Minerais (CPRM) for funding the surveys on the Negro River. Data set is available on GitHub (https://github.com/ASMontazem/Wavelet-segmentations).

References

Alsdorf, D. E., & Lettenmaier, D. P. (2003). Tracking fresh water from space. *Science*, *301*(5639), 1491–1494. https://doi.org/10.1126/science.1089802

Biancamaria, S., Lettenmaier, D. P., & Pavelsky, T. M. (2016). The swot mission and its capabilities for land hydrology. *Surveys in Geophysics*, *37*(2), 307–337. https://doi.org/10.1007/s10712-015-9346-y

Brisset, P., Monnier, J., Garambois, P.-A., & Roux, H. (2018). On the assimilation of altimetric data in 1d saint venant river flow models. *Advances in Water Resources*, *119*, 41–59. https://doi.org/10.1016/j.advwatres.2018.06.004

Calmant, S., & Seyler, F. (2006). Continental surface waters from satellite altimetry. *Comptes Rendus Geoscience*, *338*, 1113–1122. https://doi.org/10.1016/j.crte.2006.05.012, la Terre observée depuis l'espace observing the Earth from space.

Chow, V. (1959). *Open-channel Hydraulics*. New-York, USA: Mc Graw-Hill.

Domeneghetti, A., Schumann, G.J.-P., Frasson, R. P. M., Wei, R., Pavelsky, T. M., Castellarin, A., Brath, A., & Durand, M. T. (2018). Characterizing water surface elevation under different flow conditions for the upcoming SWOT mission. *Journal of Hydrology*, *561*, 848–861. https://doi.org/10.1016/j.jhydrol.2018.04.046

Frasson, R. P. M., Wei, R., Durand, M., Minear, J. T., Domeneghetti, A., Schumann, G., et al. (2017). Automated river reach definition strategies: Applications for the Surface Water and Ocean Topography mission. *Water Resources Research*, *53*, 8164–8186. https://doi.org/10.1002/2017WR020887

Garambois, P.-A., Calmant, S., Roux, H., Paris, A., Monnier, J., Finaud-Guyot, P., et al. (2017). Hydraulic visibility: Using satellite altimetry to parameterize a hydraulic model of an ungauged reach of a braided river. *Hydrological Processes*, *31*(4), 756–767. https://doi.org/10.1002/hyp.11033

Garambois, P.-A., & Monnier, J. (2015). Inference of effective river properties from remotely sensed observations of water surface. *Advances in Water Resources*, *79*, 103–120. https://doi.org/10.1016/j.advwatres.2015.02.007

Larnier, K. (2010). Modélisation thermohydraulique d'un troncon de garonne en lien avec l'habitat piscicole: approches statistique et déterministe (PhD thesis), Toulouse.

Mallat, S. (2008). *A Wavelet Tour of Signal Processing Third Edition: The Sparse Way* (3rd ed.). Orlando, FL, USA: Academic Press, Inc.

Meade, R. H., Rayol, J. M., Da Conceicão, S. C., & Natividade, J. R. G. (1991). Backwater effects in the amazon river basin of brazil. *Environmental Geology and Water Sciences*, *18*(2), 105–114. https://doi.org/10.1007/BF01704664

Moreira, D. M., Calmant, S., Perosanz, F., Xavier, L., Rotunno Filho, O. C., Seyler, F., & Monteiro, A. C. (2016). Comparisons of observed and modeled elastic responses to hydrological loading in the amazon basin. *Geophysical Research Letters*, *43*, 9604–9610. https://doi.org/10.1002/2016GL070265

O'Loughlin, F., Trigg, M. A., Schumann, G. J.-P., & Bates, P. D. (2013). Hydraulic characterization of the middle reach of the congo river. *Water Resources Research*, *49*, 5059–5070. https://doi.org/10.1002/wrcr.20398

Rodriguez, E. (2012). SWOT science requirements document. JPL document, JPL.

Samuels, P. G. (1989). Backwater llength in rivers. *Proceedings of the Institution of Civil Engineers*, *87*, 571–582.

Simeoni-Sauvage, S. (1999). Modélisation hydrobiogélochimique de la garonne a l'éltiage estival: cas de l'azote entre toulouse et agen (120 kilomèltres) (PhD thesis), INPT, Toulouse.

Torrence, C., & Compo, G. P. (1998). A practical guide to wavelet analysis. *Bulletin of the American Meteorological Society*, *79*(1), 61–78. https://doi.org/10.1175/1520-0477(1998)079<0061:APGTWA>2.0.CO;2